ACS MATERIALS Au
AN OPEN ACCESS JOURNAL OF THE AMERICAN CHEMICAL SOCIETY

pubs.acs.org/materialsau

Article

Electrophoretic Deposition of Nanocrystalline Calcium Phosphate Coating for Augmenting Bioactivity of Additively Manufactured Ti-6Al-4V

V. M. Suntharavel Muthaiah, Monika Rajput, Ananya Tripathi, Satyam Suwas, and Kaushik Chatterjee*

Cite This: *ACS Mater. Au* 2022, 2, 132–142

Read Online

ACCESS | Metrics & More | Article Recommendations

ABSTRACT: Additive manufacturing (AM) is being widely explored for engineering biomedical implants. The microstructure and surface finish of additively manufactured parts are typically different from wrought parts and exhibit limited bioactivity despite the other advantages of using AM for fabrication. The aim of this study was to enhance the bioactivity of selective laser melted Ti-6Al-4V alloy by electrophoretic deposition of nanohydroxyapatite (nanoHAp) coatings. The deposition parameters were systematically investigated after the coatings were deposited on the as-manufactured surface or after polishing the surface of the additively-manufactured sample. The surfaces were coated with nanoHAp suspended in either ethanol or butanol using different voltages (10, 30, or 50 V) for varied deposition times. The formation of the nanoHAp coating was confirmed by Fourier-transform infrared spectroscopy and X-ray diffraction. Microstructural analysis revealed that several conditions of the coating led to crack formation. The coated samples were subsequently heat-treated to improve the integrity of the coating. Heat treatment led to crack formation in several conditions due to thermal shrinkages. Coatings prepared using butanol were more uniform and had minimal cracks compared with the use of ethanol. Nanoindentation confirmed good stability and integrity of the nanoHAP coatings on the as-manufactured and polished surfaces. The coating on the as-manufactured sample exhibited higher hardness and lower elastic modulus as compared with the coating on the polished sample. *In vitro* study revealed that the nanoHAp coating markedly enhanced the attachment, proliferation, and differentiation of preosteoblasts on the alloy. These results provide a viable route to enhancing the bioactivity through deposition of nanoHAp with important implications for engineering additively manufactured orthopedic and dental implants suitable for better clinical performance.

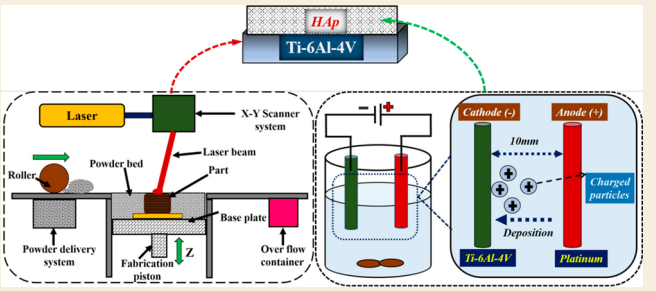

KEYWORDS: *Ti-6Al-4V, hydroxyapatite, surface modification, orthopedic biomaterials, 3D printing*

1. INTRODUCTION

Additive manufacturing (AM) or three-dimensional (3D) printing is rapidly emerging as a popular manufacturing technique for a wide variety of applications, including biomedical implants and specialty parts for the automotive and aerospace sectors, among others.[1−5] AM offers several advantages, such as the ability to manufacture complex shapes and part customization, along with a low buy-to-fly ratio. Selective laser melting (SLM) has emerged as the most mature metal-based AM technique that affords the fabrication of the desired parts from a 3D computer model by fusing metal powder particles together in a layer-by-layer method using a laser.[5] Selective laser melting (SLM) and electron beam melting (EBM) utilize powder feed for metal additive manufacturing, but there are significant differences in the interaction mechanisms between the powder and the energy source as well as the associated parameters and features, environment, and resultant properties.[6] The main advantages of SLM as an AM process include the ability to use a wider variety of materials, the ability to tune properties during the processing of the parts, increased functionality, relatively lower cost, and the production of near-net-shaped components ready to use (if the surface roughness levels are acceptable).[7] In EBM, the optimization of the process parameters is more difficult than the SLM process, and hence, only limited materials are processed by EBM.[8] The electron beam may be used multiple times to heat the powder bed and then to melt the parts selectively. In addition, the entire chamber becomes so hot after the building process that it may require

Received: September 3, 2021
Revised: November 4, 2021
Accepted: November 8, 2021
Published: November 22, 2021

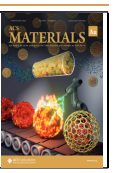

https://doi.org/10.1021/acsmaterialsau.1c00043
ACS Mater. Au 2022, 2, 132–142

Table 1. Conditions Used for the EPD Process

					quality of coating (EPD)	
substrate (Ti-6Al-4V)	solvent	HAp (g)	voltage (V)	time (min)	post-drying	heat-treated
polished	ethanol	1.0	10	2	without crack	without crack
			30			crack initiated
			50			
		2.0	10	5	deposited layer contained crack	———
			30			
			50			
	butanol	1.0	10	5	deposited layer not proper	———
			30			
			50			
		2.0	10	2	deposited layer contained without crack	deposited layer contained without crack
			30			
			50			crack initiated
as-manufactured	ethanol	1.0	10	2	good	———
			30		deposited layer contained crack	
			50			
		2.0	10		———————	
			30			
			50			
	butanol	1.0	10			
			30			
			50			
		2.0	10	2	without crack	without crack
			30			
			50			

considerable cooling time before the parts can be removed from the substrate plate.

Titanium and its alloys such as Ti-6Al-4V are widely used for manufacturing various orthopedic and dental implants approved for clinical use, owing to their good combination of mechanical properties (such as low elastic modulus, high specific strength, and fatigue strength), excellent high corrosion resistance, and good biocompatibility.[5,9,10] In contrast to other biomedical alloys such as Co−Cr and 316L stainless steel, the lower modulus of elasticity of Ti-6Al-4V is attractive to minimize stress shielding and enhance osseointegration.[11,12] However, the bioactivity of the alloy surface is limited, which has motivated the development of several surface modification strategies for Ti-6Al-4V to stimulate the biological response for osseointegration. Hydroxyapatite (HAp), a principal constituent of the human bone, has been widely used as a coating material and in other biomedical applications.[13−15] More recent research has demonstrated that nanocrystalline HAp (nanoHAp) is more effective than its bulk form.[16,17]

Surface modification of Ti-6Al-4V with nanoHAp particles offers several benefits. It minimizes the mismatch in the modulus of elasticity, thereby eliminating the stress shielding effect between implant and bones significantly. Peri-implant bone healing is enhanced by minimizing the foreign body response. Different methods have been investigated for coating bioceramics on metallic substrates such as plasma spraying process,[18,19] thermal spraying,[20] sputter coating,[21] pulsed laser ablation,[22] dynamic mixing,[23] dip coating,[24] sol−gel,[25] electrophoretic deposition,[26] magnetron sputter deposition,[27] micro-arc oxidation,[28] biomimetic coating,[29] ion-beam-assisted deposition,[30] and hot isostatic pressing.[31]

Electrophoretic deposition (EPD) is recognized as a promising method to produce homogeneous bioceramic coatings of varying thicknesses on metallic implants. In EPD, ceramic nanoparticles dispersed in alcohol are deposited as a thin layer on the metallic surface that is used as an electrode under an applied electric field. The quality of the coating depends upon several factors, such as the applied voltage, deposition time, suspension concentration, and the condition of the substrate. EPD has been used to deposit nanoHAp on different Ti alloys, and the role of different parameters has been studied. Bartmanski et al.[32] coated Ti-13Zr-1Nb alloy with nanoHAp to yield coatings that were homogeneous and thick (2 to 29 μm), with high hardness (0.0201 GPa) and Young's modulus (4.58 GPa) along with good adhesion strength. In other studies, nanoHAp particles were coated on commercially pure Ti by EPD[33,34] Yamashita et al.[35] revealed that particle size plays an important role in EPD by influencing the mobility of the charged particles. The colloidal stability of the suspension in EPD is believed to be a critical parameter for obtaining a uniform coating with good adhesion strength.[36] The roughness of the underlying substrate is important in EPD, with several studies describing that smoother surfaces (Ra ≈ 15 to 20 nm) yielded better coatings than rougher surfaces (Ra ≈ 130 to 150 nm).[37]

Several studies have been reported in the literature on wrought Ti-6Al-4V and other Ti-alloys coated with nanoHAp for biomedical applications, as described above. However, there is little reported literature on the preparation of nanoHAp coatings on additively manufactured parts of Ti-alloys such as Ti-6Al-4V and other alloys. AM results in nonequilibrium microstructures distinct from alloys prepared by conventional manufacturing. The surface roughness of AM parts tends to be high, and in parts with complex geometry, it may not even be possible to smoothen the surface postmanufacturing.

The primary objective of the present work was to assess the potential of using EPD to deposit nanoHAp coatings on

https://doi.org/10.1021/acsmaterialsau.1c00043
ACS Mater. Au 2022, 2, 132−142

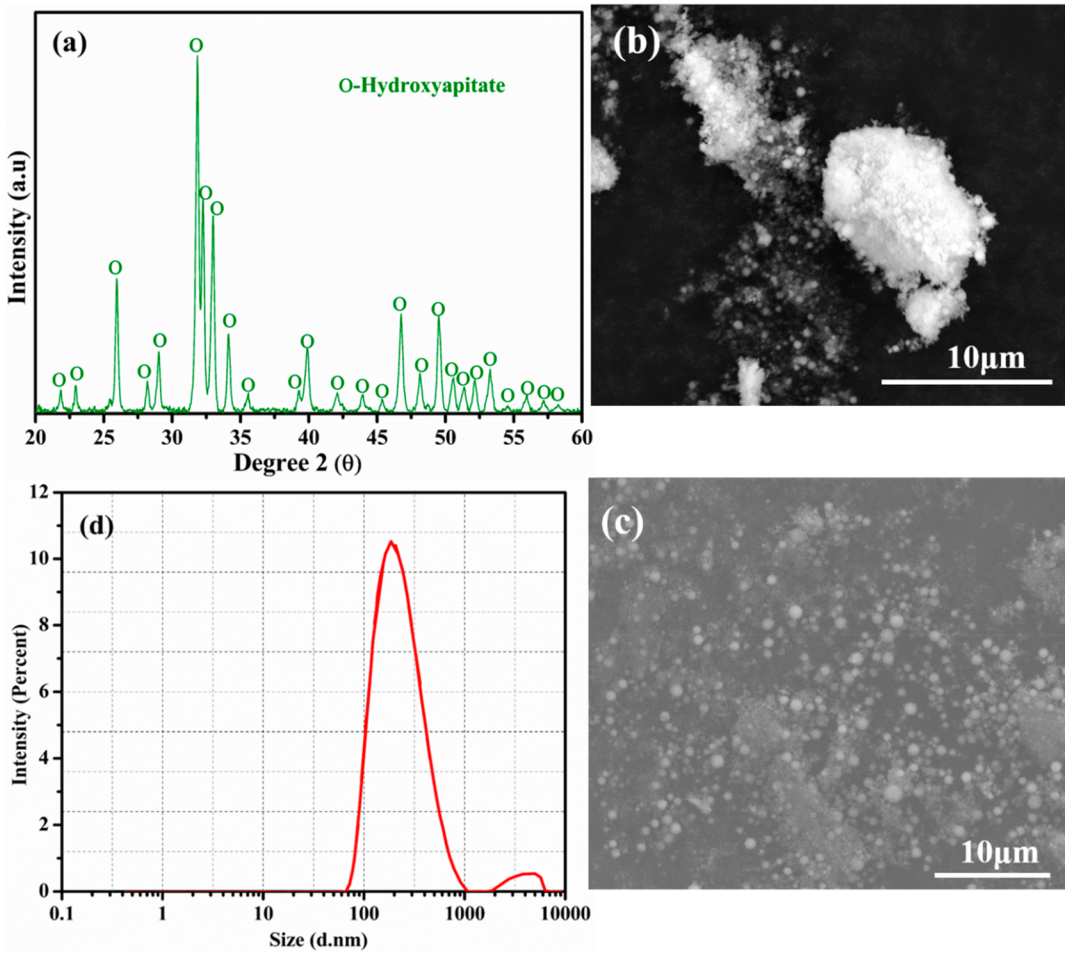

Figure 1. (a) XRD pattern of nanohydroxyapatite (HAp) powder. SEM micrographs of nanoHAp powder (b) as-received and (c) after ultrasonication for 1 h; (d) plot showing the distribution of the size of the powder determined from dynamic light scattering after ultrasonication for 1 h in ethanol suspension.

additively manufactured Ti-6Al-4V substrates toward enhancing their potential for biomedical applications. The deposition was performed on the alloy surface after SLM or after polishing the additively manufactured alloy. Different parameters controlling the EPD process, such as the choice of solvent, nanoHAp content, applied voltage, and deposition time, were systematically investigated to reveal the effects on physical properties of the nanoHAp coating and the resultant change in the cellular response to additively manufactured Ti-6Al-4V.

2. EXPERIMENTAL DETAILS

2.1. Preparation of Ti-6Al-4V Alloys

Ti-6Al-4V parts were fabricated by SLM at Intech Additive Solutions, Bangalore, using process parameters to obtain high-density blocks, as reported earlier.[38,39] Wire cut EDM (electrical discharge machining) was used to prepare samples of 1 mm thickness, 7 mm height, and 7 mm width. Samples were used with the surface in as-manufactured condition or after polishing. Samples were polished using 800 ǂ grit size silicon carbide abrasive paper. The polished and as-manufactured samples were cleaned with ethanol and then ultrasonically cleaned (Sonic-3, POLSONIC) in ethanol and distilled water for 15 min. The samples were kept in a vacuum desiccator until further processing to minimize oxide formation.

2.2. Electrophoretic Deposition of nanoHAp Coatings

A suspension of nanoHAp (Sigma-Aldrich) with an average particle size of 200 nm and spherical shape was used for EPD. The particle size was determined using dynamic light scattering (Malvern Instruments) in an ethanol suspension. The suspensions were prepared by ultrasonication and magnetic stirring for 1 h at room temperature (≈ 25 °C). Ti-6Al-4V was used as the cathode and platinum as the anode or counter electrode. Both electrodes were placed vertically parallel to each other at a distance of 1 cm. The whole setup was powered using DC power (DIGILOG Instruments). The EPD was performed on as-manufactured and polished surfaces. Table 1 compiles the different conditions used for the EPD process. The suspension was stirred continuously using the magnetic stirrer at 300 rpm during EPD. After the deposition, the samples were dried in air for 48 h at room temperature.

2.3. Heat Treatment of nanoHAp Coated Ti-6Al-4V Alloys

To enhance the bonding of the deposited coating to the underlying substrate, nanoHAp-coated samples were thermally treated in a tubular furnace (Digiqual Systems) in an argon atmosphere. The furnace was heated at 5 °C/min up to 800 °C and held for 2 h and then cooled to room temperature by switching off the furnace.

2.4. Structure and Morphology of nanoHAp Coatings

The microstructure of the naoHAp coating was analyzed using a scanning electron microscope (SEM, ULTRA 55 Carl Zeiss) with a LED detector operated at 20 kV. The phase identification was performed by X-ray diffraction analysis (XRD Philips X'Pert Pro) with monochromatized Cu Kα radiation at a scan rate of 0.02°/s in the 2θ range of 10° to 90°. Fourier-transform infrared (FTIR) spectroscopic analysis was done with a spectrophotometer (PerkinElmer Frontier) at a resolution of 2 cm^{-1} in the range of 400 to 4000

https://doi.org/10.1021/acsmaterialsau.1c00043
ACS Mater. Au 2022, 2, 132−142

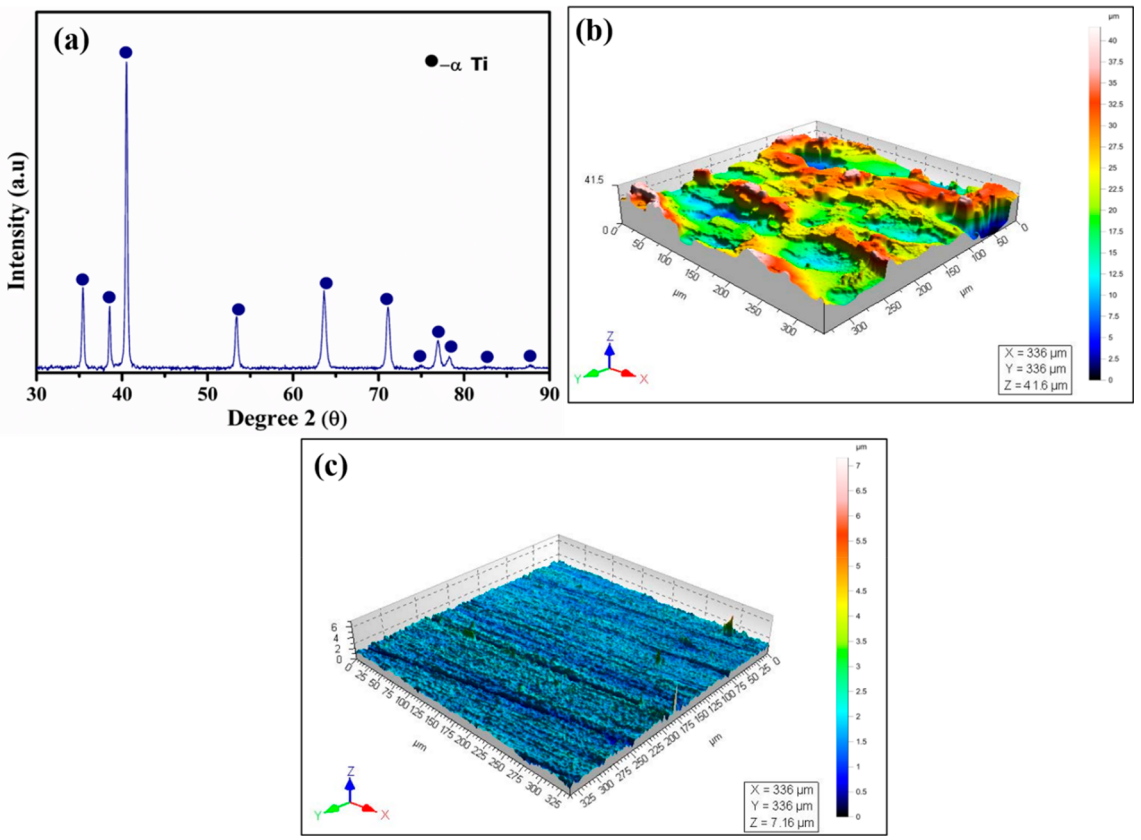

Figure 2. (a) XRD pattern of Ti-6Al-4V prepared by SLM, (b) 3D profilometer images of as-manufactured, and (c) polished Ti-6Al-4V surfaces.

cm^{-1}. The surface roughness and topography were studied at the microscale using an optical profilometer (Taylor Hobson/Talysurf CCI) over a 0.25 mm^2 area. The surface roughness parameters (R_a surface roughness, R_q root mean square deviation, R_{sk} skewness, and R_{ku} kurtosis) were calculated by using the inbuilt application tools. An atomic force microscope (AFM, Bruker, Dimension ICON) was used to study the surface topography at the nanoscale.

2.5. Mechanical Properties

Nanoindentation tests were carried out with the Nanotriboindenter TI-950 system (Hysitron Inc.) to study the adhesion characteristics of the nanoHAp coatings on the substrate using a Berkovich three-sided pyramidal diamond. For each sample, five measurements were taken. The maximum applied load was kept equal to 5 mN, the loading and unloading time was set at 20 s, and the dwell time at maximum load was 10 s. For each sample, the load−displacement curves were obtained during the indentation. The values of surface hardness (H) and Young's modulus (E) were calculated from the load−displacement plots using the in-built software. The value of Poisson's ratio was assumed to be 0.3 for determining the value of E.

2.6. *In Vitro* Cytocompatibility

Cytocompatibility of the nanoHAp coated alloy was determined by culturing MC3T3-E1 cells (ATCC). Cells were cultured on the as-manufactured samples as well on samples after polishing (without nanoHAp) as controls. Samples were cut into dimensions of 7 mm × 7 mm with a thickness of 1 mm for cell studies. In this experiment, samples were designated as follows: as-manufactured samples without nanoHAp (*as-manufactured*), polished without nanoHAp (*polished*), as-manufactured with nanoHAp coating (*as-manufactured nanoHAp*), and polished with nanoHAp coating (*polished nanoHAp*). All samples were sterilized by ultraviolet radiation for 1 h on each side in a laminar hood and incubated in minimum essential medium Eagle - alpha modification (α-MEM) media for 1 h before cell seeding.

The Alamar Blue assay (ThermoScientific) was used to quantify the cell viability of MC3T3-E1 cells on the samples. First, 3×10^3 cells were seeded per sample directly onto the metal samples in 48-well plates and incubated at 37 °C in a CO_2 incubator for attachment and proliferation. To evaluate cell viability, samples from days 1, 4, and 7 were washed with PBS and incubated in a medium containing 1 mg/mL Alamar Blue, resazurin dye for 3 h. The fluorescence of the reduced resazurin was recorded with a spectrophotometer (Biotek) at 530/590 nm. The measurements were done in triplicates.

To visualize cell morphology on the different substrates, the cells were seeded and cultured for 1, 4, or 7 days, as above. The cells were washed with 1× PBS and fixed with 3.7% formaldehyde at room temperature for 15 min. 0.1% Triton X-100 was added for 10 min to permeabilize the cell membrane. Samples were incubated in 10 μg/mL fluorescein isothiocyanate (FITC)-conjugated phalloidin (ThermoFisher) for 40 min at room temperature, followed by incubation in 1 μg/mL of 4,6-diamidino-2-phenylindole (DAPI, Sigma) for 5 min. Lastly, each step was followed by 1× PBS washing. Finally, the samples were visualized for F-actin and nuclei staining using an inverted epi-fluorescence microscope (Olympus).

3. RESULTS AND DISCUSSION

3.1. Characterization of nanoHAp

Figure 1 shows the XRD pattern of the nanoHAp, which confirms the pure hexagonal close packed structure (HCP) of the powder, corroborating results reported in the literature.[32] The XRD peaks typical of crystalline hydroxyapatite (HAp, PDF 00-009-0432) and the titanium alloy (Ti, PDF 00-044-1294) Ti-6Al-4V substrate are present. SEM micrographs of the as-received nanoHAp powder and after ultrasonication for 1 h are shown in Figure 1b,c. Figure 1d shows the dynamic light scattering measurement results of the nanoHAp powder after ultrasonication. Significant agglomeration of particles in the as-received nanoHAp was markedly reduced after ultrasonication. Ethanol or butanol was used as solvents in the

https://doi.org/10.1021/acsmaterialsau.1c00043
ACS Mater. Au 2022, 2, 132−142

present study for the purpose of ultrasonication in order to control the particle size in the narrow range and to maintain the coating integrity.[41] DLS measurements presented in Figure 1d further confirm the narrow distribution of particle size after ultrasonication. The mean size of particles is ≈200 nm, and the particles are spherical. Boccaccini et al.[43] indicated that nanoHAp particles disperse well in suspension with high mobility for facilitating uniform deposition on the surface of metallic substrates.

3.2. Characterization of Ti-6Al-4V Prepared by SLM

Figure 2a shows the XRD pattern of Ti-6Al-4V prepared by SLM, displaying peaks ($10\bar{1}0$, 0002, $10\bar{1}1$, $10\bar{1}2$, $11\bar{2}0$, $10\bar{1}3$, $20\bar{2}0$, $11\bar{2}2$, $20\bar{2}1$, $20\bar{2}2$) characteristic of the α' phase. We and others have observed the α' phase for Ti-6Al-4V prepared by SLM.[38−40,42] The body centered cubic (BCC) β-phase was not detected in the as-manufactured samples. The observed HCP pattern can be attributed to both the α phase and the α' martensite since they have the same crystalline structure and similar lattice parameters. It is reported that the high cooling rate during SLM induces precipitation of a higher amount of the α' martensite phases on Ti-6Al-4V alloy.[44] Figure 2b,c show the optical profilometer micrographs of the as-manufactured alloy surface and after polishing. The surface of the as-manufactured sample contains significant irregularities as compared with the polished surfaces. The roughness parameters associated with the surface plots (R_a: surface roughness, R_q: root mean square deviation, R_{sk}: skewness, and R_{ku}: kurtosis) are compiled in Table.2. The parameters R_a and R_q primarily reflect the average size of surface features determined by the peak heights and valley depths. The predominance of peaks (positive R_{sk}) or valleys (negative R_{sk}) is measured by the parameter R_{sk}, whereas the parameter R_{ku} represents the sharpness of the surface peaks. The values of R_a are estimated to be 1.40 and 0.195 μm for the as-manufactured and polished surfaces, respectively. Thus, the surface roughness of the polished samples is about 7 times lower than that of the as-manufactured surface. The values of R_a and R_q are also smaller after polishing. The surface skewness (R_{sk}) values for the as-manufactured and polished surfaces are +0.131 and −0.772, respectively. Thus, thin scratches are only present as a result of surface polishing, as shown in Figure 2c. The values of R_{ku} for the as-manufactured, and the polished surfaces are 5.18 and 8.05, respectively. The high positive kurtosis indicates that the surfaces have high peaks and high valleys. It has been reported by others that the choice of the surface finishing technique determines the change in surface roughness parameters of titanium surfaces[45]

Table 2. Surface Roughness Parameters of the Ti-6Al-4V Alloy

parameter	as-manufactured	post-polishing
R_a	1.40 μm	0.195 μm
R_q	1.76 μm	0.260 μm
R_{sk}	0.131	−0.772
R_{ku}	5.81	8.05

3.3. Characterization of the Coating after EPD

Figure 3 compiles the XRD patterns of surfaces coated with nanoHAp for the different conditions of EPD. The patterns show the characteristic peaks of Ti-6Al-4V and nanoHAp. Some of the samples, such as those where 30 or 50 V was applied for deposition, exhibit more prominent nanoHAp peaks than the other samples. These differences are likely because of the differences in the thickness of the coating. Bartmanski et al.[32] reported similar findings where they observed that the X-rays penetrated into the underlying substrate when the thickness and density of the coating were low.

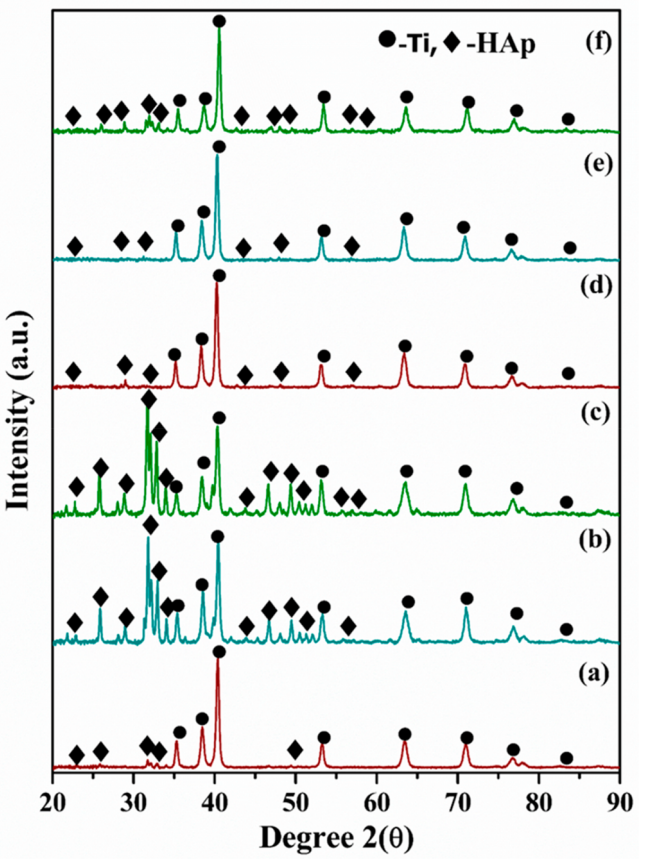

Figure 3. XRD patterns of polished samples coated with nanoHAp in (a−c) ethanol suspension ((a) 10 V, (b) 30 V, (c) 50 V). (d−f) butanol suspension ((d) 10 V, (e) 30 V, (f) 50 V) at different voltages.

Figure 4 shows the FTIR spectra of the as-manufactured Ti-6Al-4V substrate coated with nanoHAp in butanol suspension at different voltages. The characteristic bonds associated with the different peaks are indicated in the spectra. The peak at 3750 cm^{-1} corresponds to the P−OH groups of nanoHAp, whereas the peaks observed at 2870 and 2940 cm^{-1} indicate the stretching vibration of C−H bonds. The peak at 1038 cm^{-1} indicates the formation of phosphate groups (PO_4^{3-}), and the peaks around 1420, 1450, and 873 cm^{-1} belong to the carbonate groups (CO_3^{2-}). These observations indicate that molecules rich in −OH functional groups can adsorb to the P−OH groups on the surface through hydrogen bonding. Morteza et al.[46] reported similar observations for butanol, ethanol, methanol, and isopropyl alcohol with HAp powder. In addition, they reported that the surface P−OH groups of HAp favor interactions with H_2O, CO_2, CH_3OH, pyridine, *n*-butylamine, triethanolamine, and acetic acid through hydrogen bonding.

Figure 5 presents the microstructures of the nanoHAp coatings on the as-manufactured and polished Ti-6Al-4V surfaces prepared by EPD with different conditions (voltage

https://doi.org/10.1021/acsmaterialsau.1c00043
ACS Mater. Au 2022, 2, 132−142

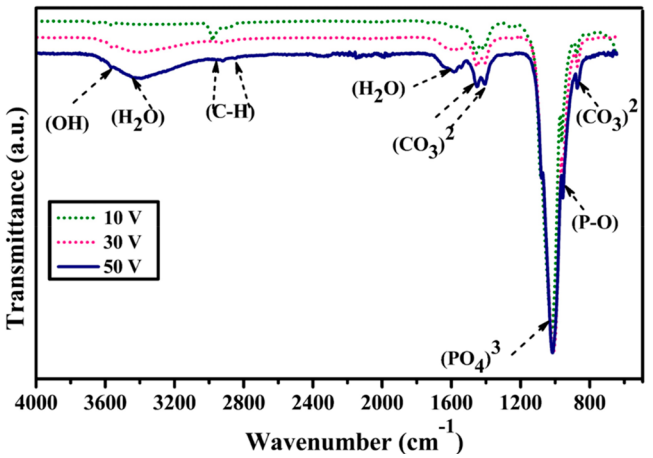

Figure 4. FTIR spectra of as-manufactured Ti-6Al-4V alloy substrate coated with nanoHAp at different voltages

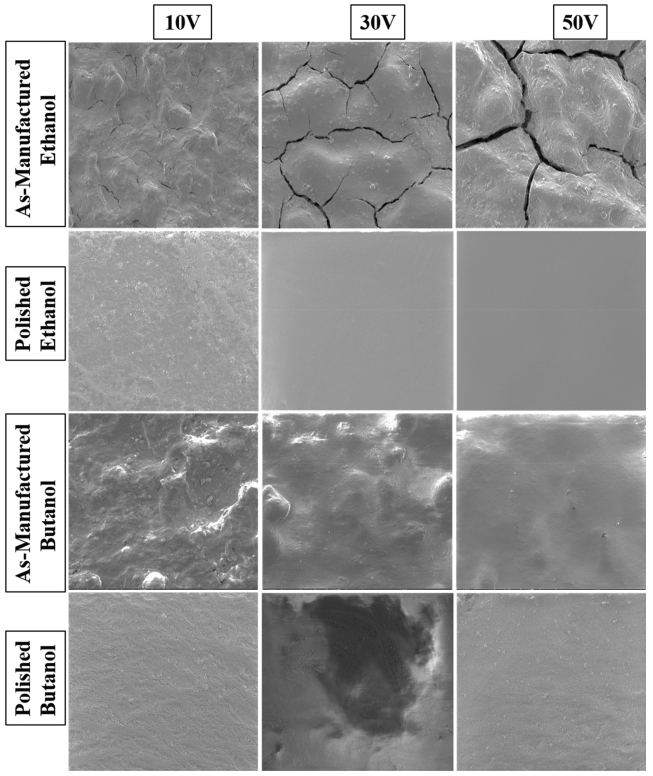

Figure 5. Scanning electron micrographs of nanoHAp coating on as-manufactured and polished Ti-6Al-4V deposited by EPD for 2 min at different voltage and solvent conditions. Scale bar = 100 μm.

and solvent) for a fixed deposition time of 2 min. It can be observed that an increase of voltage (from 10 to 50 V) led to the formation of coatings with an increased propensity for cracking due to shrinkage of the coating during drying. Intense cracking in the coatings deposited from suspensions of alcohol of small molecular size tends to occur because of their higher shrinkage during drying resulting from their larger thickness. If the surface roughness of the substrate is more, it can lead to stress concentration and crack propagation in the coating. Interfacial stresses can arise at the interface because of the difference in the structure and properties between the coating and the underlying substrate, and thus, only optimal process parameters can result in the deposition of crack-free coatings. Coatings prepared using ethanol were more prone to cracking than those prepared with butanol. As ethanol has a lower boiling point and higher vapor pressure than butanol, the drying process can result in crack formation.[46] Goryczka et al.[47] showed that either deposition time or applied voltage could be altered to change the thickness of the HAp coating. The polished samples coated with nanoHAp show smoother surfaces with minimal visible pores or cracks at higher applied voltages. The formation of cracks may occur because of the higher thickness of the coating and the faster mobility of ions in ethanol suspension compared to the butanol suspension at lower deposition time.[32] The coatings were smoother and more uniform when butanol was used as the solvent due to the lower mobility of ions in butanol. With butanol suspensions, coating on the as-manufactured surfaces at the lower voltage (10 V) revealed some agglomeration and unevenness on the surface. At increased voltage (30 and 50 V), the coatings appear smoother. This is possibly due to the high concentration of nanoHAp particles in butanol suspension, which allows them to migrate rapidly at lower voltages, forming more homogeneous coatings on the substrate. Taken together, butanol is better than ethanol in yielding uniform coatings of nanoHAp particles on Ti-6Al-4V. Yildirim et al.[48] showed that higher voltage and short deposition time are better suited for coating of nanoHAp on metallic substrates as compared with the deposition of the micron-sized particles. In another study, Rojaee et al.[49] observed the surface roughness of the substrate significantly influences the coating morphology and integrity. Bartmanski et al.[32] showed that the increase of nanoHAp powder in the suspension and applied voltage increase the density of the coating, possibly because of the faster migration of nanoparticles.

Figure 6 presents the images obtained from the profilometer for the nanoHAp-coated surfaces of the as-manufactured and polished samples for different deposition conditions. The thickness of the coatings in both ethanol and butanol suspensions was observed to increase with an increase in the

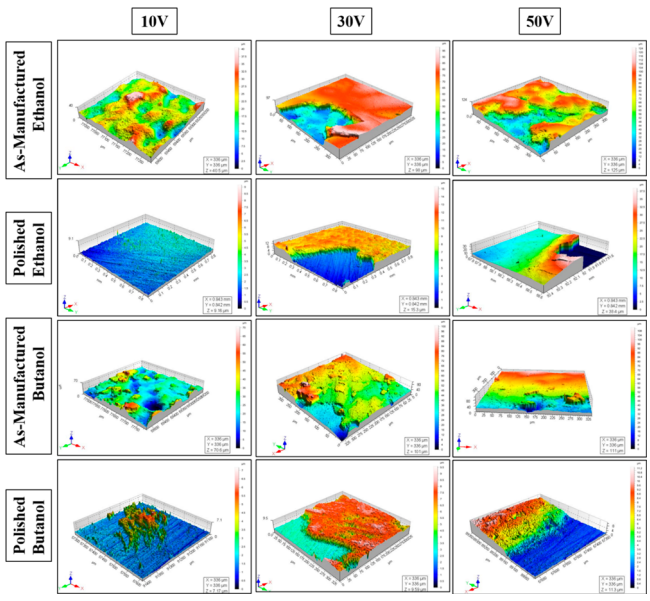

Figure 6. 3D profilometer images of as-manufactured and polished Ti-6Al-4V alloys coated with nanoHAp at different voltages and suspensions.

https://doi.org/10.1021/acsmaterialsau.1c00043
ACS Mater. Au 2022, 2, 132−142

applied voltage. The thickness of coating attained using the EPD technique is reported to lie between 0.1 to 100 μm in different studies.[50,51] A thicker coating may lead to failure because of delamination and degradation, thereby resulting in instability of the implant and enhances the risk of implant failure. de Groot et al.[52] reported that coatings thicker than 100 μm were associated with delamination and fragmentation with poor mechanical properties, which may cause fatigue failure, poor adhesion, and quick dissolution. Thinner coatings ($\approx$ 50 μm), on the other hand, exhibit a stronger fixation with living tissues. Thinner coatings facilitate osseointegration through the interaction of bioactive HAp, a material favorable for augmenting osseointegration. The optimal thickness of HAp coatings on different metallic biomaterials is reported to be in the range of 50 to 100 μm.[53−56]

Figure 7 shows the AFM images of the polished samples coated with nanoHAP at different voltages and the two

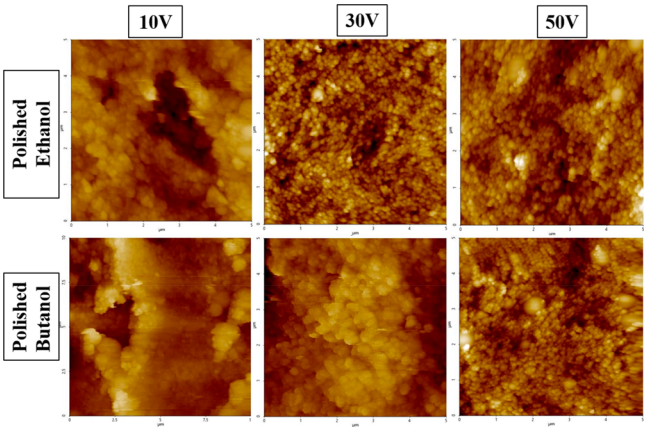

Figure 7. Atomic force micrographs of nanoHAp-coated substrates prepared at different voltages and solvents.

solvents, ethanol and butanol. The grain size of the HAp coatings over the substrate lies in the nanometer range. No agglomeration or pores are observed, and the feature sizes closely match the results of the particles from SEM and DLS (Figure 1). On the as-manufactured samples, the R_a parameter ranges from 1.18 to 1.87, whereas on the polished sample, R_a ranges from 0.22 to 0.57 at the different voltages (see values listed in Table.3) Increased roughness can enhance the water wettability for the Wenzel state.

Table 3. Surface Roughness of the Substrates

sample	surface roughness (R_a)	
as-manufactured (butanol)	10 V	1.87 μm
	30 V	1.83 μm
	50 V	1.18 μm
polished (butanol)	10 V	0.57 μm
	30 V	0.37 μm
	50 V	0.22 μm

3.4. Heat Treatment of nanoHAp Coated Substrate

Coatings prepared by EPD are often heat-treated to remove volatile species from the layer and enhance the bonding of particles in the coated layer. The Young's modulus, hardness, adhesion strength, and crystallinity of coatings are typically altered by heat treatment. Figure 8 shows the microstructures

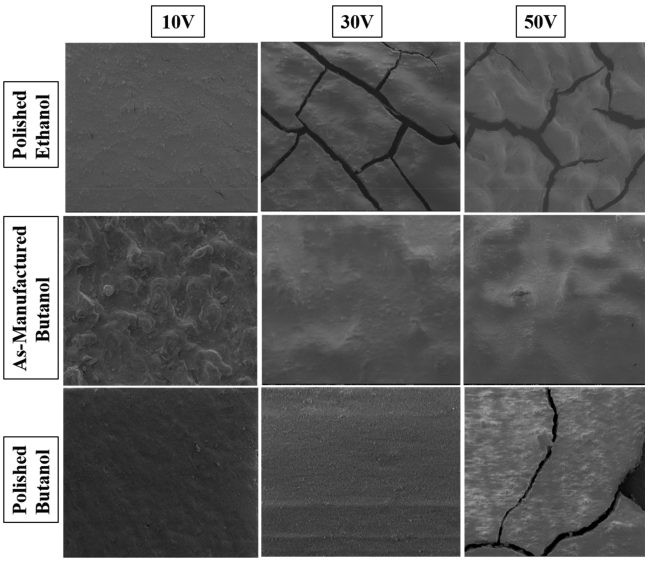

Figure 8. Scanning electron micrographs of as-manufactured and polished samples with nanoHAp coating after heat treatment at 800 °C. Scale bar = 100 μm.

of the nanoHAp-coated substrates after heat treatment at 800 °C. Figure 8 reveals a higher tendency for crack propagation with an increase in the voltage of deposition, which is ascribed to the significant shrinkage of the coating during the heat treatment. The thickness of coatings tends to increases with an increase in the voltage. The nanoHAp coating on the as-manufactured sample prepared with ethanol suspension shows several cracks that formed during drying prior to heat treatment (Figure 5). However, heat treatment of the polished samples coated with nanoHAp in ethanol suspension revealed the initiation of cracks during heat treatment itself due to shrinkage. Cracks can appear due to the mechanical stresses exerted on the coating due to shrinkages during heating at a high temperature. The crack initiation of as-manufactured and polished samples with nanoHAp coating in ethanol suspension demonstrates that this solvent is not suitable for depositing the nanoHAp layer.

The as-manufactured and polished samples with the nanoHAp coating prepared using butanol suspension show good integrity after heat treatment. Among these, the coating deposited at 50 V on the polished sample after the heat treatment shows several cracks due to shrinkage during heat treatment. The polished sample (50 V) coated with nanoHAp in butanol suspension had a coating thickness of $\approx$11.3 μm. High-temperature sintering can be utilized to minimize the porosity by increasing the coating density. However, cracks in the coating can form during sintering because of the difference in the thermal expansion coefficients between the substrate and nanoHAp and the large reduction of the pore volume. Furthermore, the success of electrophoretically deposited HAp has been limited to conventional materials in the range of micron-sized grains.[57]

Figure 9 shows the 3D profilometer images of nanoHAp-coated samples after heat treatment at 800 °C. It is seen that the thickness of the nanoHAp coating deposited with ethanol increases with an increase in the voltage. The coating thickness of the nanoHAp coated samples with different voltages and suspension are compiled in Table.4. The heat-treated nano-HAp coatings on the as-manufactured samples prepared in

https://doi.org/10.1021/acsmaterialsau.1c00043
ACS Mater. Au 2022, 2, 132−142

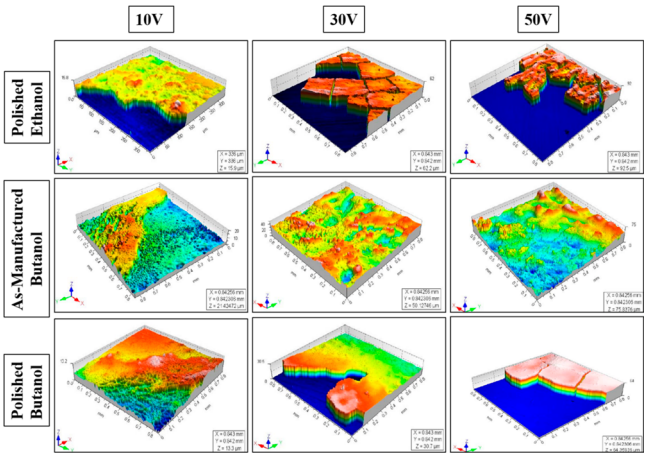

Figure 9. 3D profilometer micrograph of nanoHAp coated samples after heat treatment.

Table 4. Coating Thickness before and after Heat Treatment

samples	solvent	voltage (V)	thickness after EPD (μm)	thickness after heat treatment (μm)
as-manufactured	ethanol	10	40.5	cracks
		30	98.0	cracks
		50	125.0	cracks
polished	ethanol	10	9.16	15.9
		30	15.3	62.2
		50	38.4	92.5
as-manufactured	butanol	10	10.8	21.4
		30	15.3	50.1
		50	38.4	75.8
polished	butanol	10	7.17	13.3
		30	9.53	30.7
		50	11.3	64.3

butanol indicate better integrity without cracks. The EPD process of nanoHAP particles leads to the mechanical interlocking of particles with the substrate, and it helps to achieve better mechanical properties such as adhesion and fatigue and corrosion resistance. Morteza et al.[46] reported that after the heat treatment, many small cracks were observed on coated surfaces prepared using the EPD process because of the evaporation of solvent trapped within the coating and the difference in thermal expansion coefficients between the substrate and the coating. Bartmanski et al.[32] observed formation of of cracks due to significant shrinkage of the coating at a higher sintering temperature.

Figure 10 shows the load−displacement curves of the nanoHAp-coated surfaces prepared using butanol after the heat treatment. Young's modulus and hardness determined from the plots are tabulated in Table 5. Table 5 reveals a steady increase in hardness with decreasing thickness of the nanoHAp coating and increasing voltage used for EPD. Nanoindentation measurements performed in cross-section at the interface of the metal-ceramic coating revealed a hardness of 2 GPa and a Young's modulus of 80 GPa. These results are in good agreement with the work of Saber-Samandari et al., who performed nanoindentation measurements of HAp coatings deposited on Ti6Al4V.[58] The coatings on the as-manufactured samples show a higher hardness and a lower elastic modulus value as compared with the polished samples.

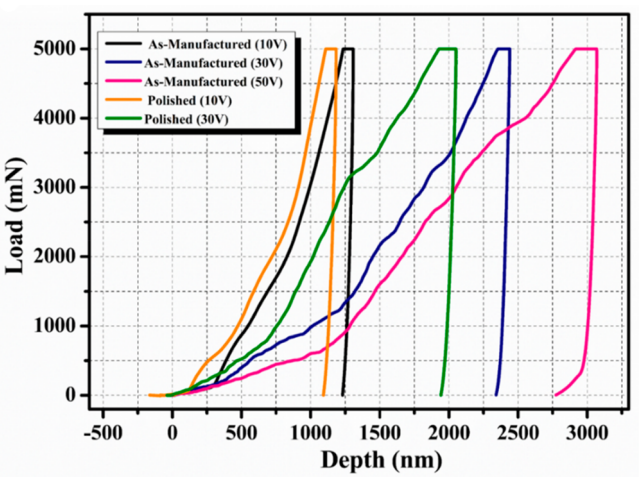

Figure 10. Representative load vs displacement plots obtained from the nanoindentation test for nanoHAp-coated surfaces after heat treatment of coating prepared by EPD using butanol

The superior result likely arises because of the higher bulk density and lower thickness of the coating. Saber-Samandari et al.[58] showed that the mechanical properties of coatings are related to the interface distance from the substrate to the coating. The mechanical properties (hardness and Young's modulus values) increase gradually with distance from the substrate, with a steeper gradient in the coating made from smaller particles. Using the laser melting technique for HAp coatings on metallic substrates, Cheng et al.[59] showed that coating leads to an increase of hardness to 7 GPa from 2.5 GPa at the substrate. In this work, we observed a decrease in the surface hardness with an increase in the thickness of the coating.

Taken together, the results presented above on the characterization of the nanoHAp coatings prepared by EPD on additively manufactured Ti6Al4V substrates revealed that the best coatings are obtained when butanol is used as the solvent with 10 V followed by heat treatment. These coatings provide the best combination of optimal thickness for osseointegration with minimal pores or cracking. Thus, these surfaces were selected for assessing the biological response by measuring the cell response *in vitro*. The results of the EPD process here on the as-manufactured substrates without the need for polishing have important implications for depositing nanoHAp coatings on porous and lattice structures, which are being widely prepared by SLM.

3.5. Cell Response to the Coated Substrates

The attachment and viability of cells onto the as-manufactured and polished Ti-6Al-4V samples with/without nanoHAp coatings were tested with osteoblasts. The cell response was quantified with the Alamar Blue assay, as presented in Figure 11. All the tested samples were deemed to be cytocompatible as they supported the attachment and growth of the osteoblasts. No significant differences in cell growth were found at day 1 on all the samples. However, a significant difference was observed in cell growth at day 4. Cell numbers, as assumed to be proportional to the fluorescence intensity, were significantly higher on the coated samples (as-manufactured nanoHAp coated and polished nanoHAp-coated) compared to the surfaces without the coating. Thus, the cells appeared to proliferate better on the Ti-6Al-4V when coated with nanoHAp. It has already been reported that

https://doi.org/10.1021/acsmaterialsau.1c00043
ACS Mater. Au 2022, 2, 132−142

Table 5. Mechanical Properties of the nanoHAp Coated Samples[a]

	hardness (GPa)			Young's modulus (GPa)		
sample	10 V	30 V	50 V	10 V	30 V	50 V
as-manufactured	0.204 ± 0.053	0.038 ± 0.008	0.030 ± 0.008	19.15 ± 1.95	7.40 ± 1.36	6.74 ± 1.47
polished	0.163 ± 0.006	0.063 ± 0.007	-	21.28 ± 1.89	8.54 ± 1.65	-
uncoated surface		5.96 ± 1.172			151 ± 3.50	

[a]Data are shown as mean ± SD for $n = 5$.

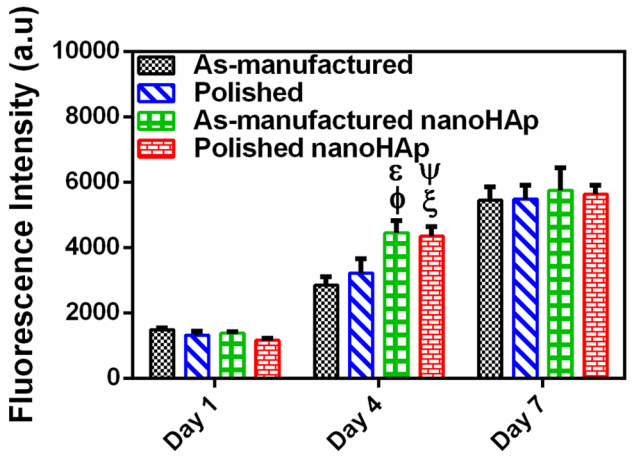

Figure 11. Plot of the fluorescence measured by Alamar Blue assay for MC3T3-E1 cells cultured onto the uncoated (as-manufactured and polished) and coated (as-manufactured nanoHAp and polished nanoHAp) surfaces. All data are mean ± SD for $n = 3$. ANOVA multiple comparison test showing significant difference $p < 0.0001$ (****) between as-manufactured vs as-manufactured nanoHAp (Φ), and as-manufactured vs polished nanoHAp (ξ); $p < 0.01$ between polished vs as-manufactured nanoHAp (γ), and polished vs polished nanoHAp (ψ) at day 4.

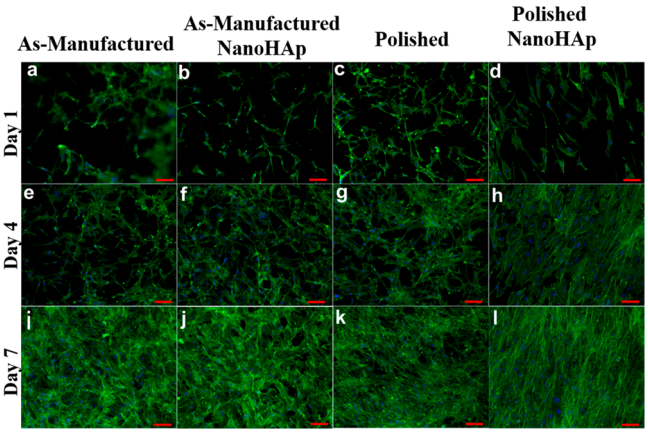

Figure 12. Fluorescence micrographs at 10× showing the morphology of MC3T3-E1 cells on the nanoHAp coated and uncoated samples stained for F-actin (green) and nuclei (blue) at days 1, 4, and 7 (Scale bar = 100 μm).

fibronectin and vitronectin are the two important proteins that influence cell attachment and proliferation.[58] The adsorption of these two proteins is favored by the presence of positively charged sites in HAp due to the presence of calcium ions.[60,37] Note that there were no discernible differences by day 7 when the cells likely reached confluency on all the surfaces.

Furthermore, the cell morphology and cytoskeletal organization of the MC3T3-E1 cells on nanoHAp coated and uncoated substrates were assessed by fluorescence microscopy, as seen in Figure 12. The cells showed well-spread morphology on nanoHAp coated surfaces (both polished and as-manufactured) in contrast to the less spread cells on the uncoated samples. Notably, F-actin was preferentially concentrated at the periphery of cells on the coated samples, whereas cells on uncoated samples showed a diffused distribution of F-actin throughout the cells.[61] These results suggest that coating of additively manufactured Ti6Al4V by EPD of nanoHAp coated markedly enhances the cytocompatibility of the alloy by augmenting the adhesion and proliferation of cells, underscoring the promise of such strategies for enhancing the clinical performance of additively manufactured implants. Notably, in earlier work with conventionally manufactured alloys, the surfaces were initially smoothened to low roughness prior to the EPD of nanoHAp.[61,62] However, we successfully prepared these coatings even on surfaces of the additively manufactured parts with markedly higher roughness. Surface engineering of additively manufactured metallic implants and specifically for titanium implants is an active area fo research.[63] These results will enable the fabrication of orthopedic implants of complex geometry, leveraging the opportunities of additive manufacturing, and their clinical performance can be augmented by coating with nanoHAp prepared by EPD.

4. CONCLUSION

The feasibility of preparing coatings of nanoHAp on additively manufactured Ti-6Al-4V alloy was studied. NanoHAp was deposited from ethanol or butanol suspensions by the EPD process followed by heat treatment. The effects of deposition parameters such as concentration, the voltage applied, and deposition time on the coating were systematically studied in detail. NanoHAp coatings of <100 μm thickness that are crack-free and uniform were successfully deposited using butanol as the solvent for preparing the suspension. Nanoindentation measurements revealed that the coating on the as-manufactured sample has higher hardness and lower elastic modulus as compared with the coating on the polished sample. Significant enhancements in osteoblast attachment, spreading, and growth were observed on the alloy surfaces coated with nanoHAp. These results have important applications for preparing high-performance next-generation orthopedic implants by additive manufacturing.

AUTHOR INFORMATION

Corresponding Author

Kaushik Chatterjee − *Department of Materials Engineering, Indian Institute of Science, Bangalore 560012, India;* orcid.org/0000-0002-7204-2926; Phone: +91-80-22933408; Email: kchatterjee@iisc.ac.in

https://doi.org/10.1021/acsmaterialsau.1c00043
ACS Mater. Au 2022, 2, 132−142

Authors

V. M. Suntharavel Muthaiah − *Department of Materials Engineering, Indian Institute of Science, Bangalore 560012, India*

Monika Rajput − *Department of Materials Engineering, Indian Institute of Science, Bangalore 560012, India*

Ananya Tripathi − *Department of Materials Engineering, Indian Institute of Science, Bangalore 560012, India*

Satyam Suwas − *Department of Materials Engineering, Indian Institute of Science, Bangalore 560012, India*

Complete contact information is available at: https://pubs.acs.org/10.1021/acsmaterialsau.1c00043

Notes

The authors declare no competing financial interest.

■ ACKNOWLEDGMENTS

The authors acknowledge the Department of Materials Engineering and Centre for Nano Science and Engineering, IISc, for access to research facilities. The authors thank Prof. Praveen Kumar for access to the nanoindenter. Support from the Department of Science and Technology (DST), Government of India (DST/NM/NB/2018/119(G)) is gratefully acknowledged.

■ REFERENCES

(1) Acharya, S.; Soni, R.; Suwas, S.; Chatterjee, K. Additive manufacturing of Co-Cr alloys for biomedical applications: A concise review. *J. Mater. Res.* **2021**, *13*, 2286−2301.

(2) Niinomi, M.; Nakai, M.; Hieda, J. Development of new metallic alloys for biomedical applications. *Acta Biomater.* **2012**, *8*, 3888−3903.

(3) Wauthle, R.; Ahmadi, S. M.; Yavari, S. A.; Mulier, M.; Zadpoor, A. A.; Weinans, H.; Van Humbeeck, J.; Kruth, J. P.; Schrooten, J. Revival of pure titanium for dynamically loaded porous implants using additive manufacturing. *Mater. Sci. Eng., C* **2015**, *54*, 94−100.

(4) Jaganathan, S. K.; Supriyanto, E.; Murugesan, S.; Balaji, A.; Asokan, M. K. Biomaterials in cardiovascular research: applications and clinical implications. *BioMed Res. Int.* **2014**, *2014*, 1−11.

(5) Zhang, X. Y.; Fang, G.; Leeflang, S.; Böttger, A. J.; Zadpoor, A. A.; Zhou, J. Effect of subtransus heat treatment on the microstructure and mechanical properties of additively manufactured Ti-6Al-4V alloy. *J. Alloys Compd.* **2018**, *735*, 1562−1575.

(6) Gokuldoss, P. K.; Kolla, S.; Eckert, J. Additive manufacturing processes: Selective laser melting, electron beam melting and binder jetting-Selection guidelines. *Materials* **2017**, *10* (6), 672.

(7) Koptyug, A.; Bäckström, M.; Botero, C.; Popov, V.; Chudinova, E. Developing new materials for electron beam melting: experiences and challenges. *Mater. Sci. Forum* **2018**, *941*, 2190−2195.

(8) Khrapov, D.; Koptyug, A.; Manabaev, K.; Léonard, F.; Mishurova, T.; Bruno, G.; Cheneler, D.; Loza, K.; Epple, M.; Surmenev, R.; Surmeneva, M. The impact of post manufacturing treatment of functionally graded Ti6Al4V scaffolds on their surface morphology and mechanical strength. *J. Mater. Res. Technol.* **2020**, *9* (2), 1866−1881.

(9) Bahl, S.; Suwas, S.; Chatterjee, K. Comprehensive review on alloy design, processing, and performance of β Titanium alloys as biomedical materials. *Int. Mater. Rev.* **2021**, *66*, 114−139.

(10) Arifin, A.; Sulong, A. B.; Muhamad, N.; Syarif, J.; Ramli, M. I. Material processing of hydroxyapatite and titanium alloy (HA/Ti) composite as implant materials using powder metallurgy: A review. *Mater. Eng.* **2014**, *55*, 165−175.

(11) Hench, L. L.; Thompson, I. Twenty-first century challenges for biomaterials. *J. R. Soc., Interface* **2010**, *7*, S379−S391.

(12) Sallica-Leva, E.; Caram, R.; Jardini, A. L.; Fogagnolo, J. B. Ductility improvement due to martensite a' decomposition in porous Ti-6Al-4V parts produced by selective laser melting for orthopedic implants. *J. Mech. Behav. Biomed.* **2016**, *54*, 149−158.

(13) Dorozhkin, S. V. Bioceramics of calcium orthophosphates. *Biomaterials* **2010**, *31*, 1465−85.

(14) Niespodziana, K.; Jurczyk, K.; Jakubowicz, J.; Jurczyk, M. Fabrication and properties of titanium-hydroxyapatite nanocomposites. *Mater. Chem. Phys.* **2010**, *123*, 160−5.

(15) Cook, S. D.; Thomas, K. A.; Kay, J. F.; Jarcho, M. Hydroxyapatitecoated porous titanium for use as an orthopedic biologic attachment system. *Clin. Orthop. Relat. Res.* **1988**, *230*, 303−312.

(16) Zhang, Z.; Dunn, M. F.; Xiao, T. D.; Tomsia, A. P.; Saiz, E. Nanostructured hydroxyapatite coatings for improved adhesion and corrosion resistance for medical implants. *MRS Proceedings* 2001, *703*. DOI: 10.1557/PROC-703-V7.5

(17) Drevet, R.; Jaber, N. B.; Fauré, J.; Tara, A.; Larbi, A. B. C.; Benhayoune, H. Electrophoretic deposition (EPD) of nano-hydroxyapatite coatings with improved mechanical properties on prosthetic Ti6Al4V substrates. *Surf. Coat. Technol.* **2016**, *301*, 94−99.

(18) De Groot, K.; Geesink, R.; Klein, C. P. A. T.; Serekian, P. Plasma sprayed coatings of hydroxyapatite. *J. Biomed. Mater. Res.* **1987**, *21*, 1375−1381.

(19) Heimann, R. B. *Plasma-Spray Coating: Principles and Applications*; John Wiley & Sons, Inc., 2008.

(20) Gross, K. A.; Berndt, C. C. Thermal processing of hydroxyapatite for coating production. *J. Biomed. Mater. Res.* **1998**, *39*, 580−7.

(21) Ding, S.-J. Properties and immersion behavior of magnetron-sputtered multi- layered hydroxyapatite/titanium composite coatings. *Biomaterials* **2003**, *24*, 4233−8.

(22) Cleries, L.; Martınez, E.; Fernandez-Pradas, J. M.; Sardin, G.; Esteve, J.; Morenza, J. L. Mechanical properties of calcium phosphate coatings deposited by laser ablation. *Biomaterials* **2000**, *21*, 967−71.

(23) Yoshinari, M.; Ohtsuka, Y.; Dérand, T. Thin hydroxyapatite coating produced by the ion beam dynamic mixing method. *Biomaterials* **1994**, *15*, 529−35.

(24) Kaciulis, S.; Mattogno, G.; Napoli, A.; Bemporad, E.; Ferrari, F.; Montenero, A.; Gnappi, G. Surface analysis of biocompatible coatings on titanium. *J. Electron Spectrosc. Relat. Phenom.* **1998**, *95*, 61−69.

(25) Li, P.; De Groot, K.; Kokubo, T. Bioactive Ca10(PO4)6-(OH)2_TiO2 composite coating prepared by sol-gel process. *J. Sol-Gel Sci. Technol.* **1996**, *7*, 27−34.

(26) Han, Y.; Fu, T.; Lu, J.; Xu, K. Characterization and stability of hydroxyapatite coatings prepared by an electrodeposition and alkaline-treatment process. *J. Biomed. Mater. Res.* **2001**, *54*, 96−101.

(27) Chudinova, E.; Surmeneva, M.; Koptioug, A.; Scoglund, P.; Surmenev, R. Additive manufactured Ti6Al4V scaffolds with the RF-magnetron sputter deposited hydroxyapatite coating. *Journal of Physics: Conference Series* **2016**, *669*, 012004.

(28) Komarova, E. G.; Sharkeev, Y. P.; Sedelnikova, M. B.; Prosolov, K. A.; Khlusov, I. A.; Prymak, O.; Epple, M. Zn-or Cu-containing CaP-based coatings formed by micro-arc oxidation on titanium and Ti-40Nb alloy: Part I—microstructure, composition and properties. *Materials* **2020**, *13* (18), 4116.

(29) Habibovic, P.; Barrere, F.; Blitterswijk, C. A.; Groot, K.; Layrolle, P. Biomimetic hydroxyapatite coating on metal implants. *J. Am. Ceram. Soc.* **2002**, *85*, 517−22.

(30) Choi, J. M.; Kim, H. E.; Lee, I. S. Ion-beam-assisted deposition (IBAD) of hydroxyapatite coating layer on Ti-based metal substrate. *Biomaterials* **2000**, *21*, 469−73.

(31) Wie, H.; Herø, H.; Solheim, T. Hot isostatic pressing-processed hydroxyapatite- coated titanium implants: light microscopic and scanning electron microscopy investigations. *Int. J. Oral Maxillofac. Implants.* **1998**, *13*, 837.

(32) Bartmanski, M.; Zielinski, A.; Majkowska-Marzec, B.; Strugala, G. Effects of solution composition and electrophoretic deposition

voltage on various properties of nanohydroxyapatite coatings on the Ti13Zr13Nb alloy. *Ceram. Int.* **2018**, *44*, 19236−19246.
(33) Abdeltawab, A. A.; Shoeib, M. A.; Mohamed, S. G. Electrophoretic deposition of hydroxyapatite coating on titanium from dimethylformamide suspensions. *Surf. Coat. Technol.* **2011**, *206*, 43−50.
(34) Ma, J.; Liang, C. H.; Kong, L. B.; Wang, C. Colloidal characterization and electrophoretic deposition of hydroxyapatite on titanium substrate. *J. Mater. Sci.: Mater. Med.* **2003**, *14*, 797−801.
(35) Yamashita, K.; Matsuda, M.; Inda, Y.; Umegaki, T.; Ito, M.; Okura, T. Dielectric depression and dispersion in electrophoretically fabricated BaTiO3 Ceramic films. *J. Am. Ceram. Soc.* **1997**, *80*, 1907−9.
(36) Zhitomirsky, I.; Gal-Or, L. Electrophoretic deposition of hydroxyapatite. *J. Mater. Sci.: Mater. Med.* **1997**, *8*, 213−9.
(37) Kumar, R. M.; Kuntal, K. K.; Singh, S.; Gupta, P.; Bhushan, B.; Gopinath, P.; Lahiri, D. Electrophoretic deposition of hydroxyapatite coating on Mg-3Zn alloy for orthopaedic application. *Surf. Coat. Technol.* **2016**, *287*, 82−92.
(38) Sabban, R.; Bahl, S.; Chatterjee, K.; Suwas, S. Globularization using heat treatment in additively manufactured Ti-6Al-4V for high strength and toughness. *Acta Mater.* **2019**, *162*, 239−254.
(39) Srinivasan, D.; Singh, A.; Reddy, A. S.; Chatterjee, K. Microstructural study and mechanical characterization of heat-treated direct metal laser sintered Ti6Al4V for biomedical applications. *Mater. Technol.* **2020**, 1−12.
(40) Zhang, X. Y.; Fang, G.; Leeflang, S.; Böttger, A. J.; Zadpoor, A. A.; Zhou, J. Effect of subtransus heat treatment on the microstructure and mechanical properties of additively manufactured Ti-6Al-4V alloy. *J. Alloys Compd.* **2018**, *735*, 1562−1575.
(41) Meng, X.; Kwon, T. Y.; Kim, K. H. Hydroxyapatite coating by electrophoretic deposition at dynamic voltage. *Dent. Mater. J.* **2008**, *27* (5), 666−671.
(42) Chudinova, E. A.; Surmeneva, M. A.; Timin, A. S.; Karpov, T. E.; Wittmar, A.; Ulbricht, M.; Ivanova, A.; Loza, K.; Prymak, O.; Koptyug, A.; Epple, M.; Surmenev, R. A. Adhesion, proliferation, and osteogenic differentiation of human mesenchymal stem cells on additively manufactured Ti6Al4V alloy scaffolds modified with calcium phosphate nanoparticles. *Colloids Surf., B* **2019**, *176*, 130−139.
(43) Boccaccini, A. R.; Zhitomirsky, I. Application of electrophoretic and electrolytic deposition techniques in ceramics processing. *Curr. Opin. Solid State Mater. Sci.* **2002**, *6* (3), 251−260.
(44) Da Silva, S. L. R.; Kerber, L. O.; Amaral, L.; Dos Santos, C. A. X-ray diffraction measurements of plasma-nitrided Ti-6Al-4V. *Surf. Coat. Technol.* **1999**, *116−119*, 342−346.
(45) Pierre, C.; Bertrand, G.; Rey, C.; Benhamou, O.; Combes, C. Calcium phosphate coatings elaborated by the soaking process on titanium dental implants: Surface preparation, processing and physical-chemical characterization. *Dent. Mater.* **2019**, *35*, e25−e35.
(46) Farrokhi-Rad, M.; Shahrabi, T. Effect of suspension medium on the electrophoretic deposition of hydroxyapatite nanoparticles and properties of obtained coatings. *Ceram. Int.* **2014**, *40*, 3031−3039.
(47) Dudek, K.; Goryczka, T. Electrophoretic deposition and characterization of thin hydroxyapatite coatings formed on the surface of NiTi shape memory alloy. *Ceram. Int.* **2016**, *42*, 19124−19132.
(48) Yildirim, O. S.; Aksakal, B.; Celik, H.; Vangolu, Y.; Okur, A. An investigation of the effects of hydroxyapatite coatings on the fixation strength of cortical screws. *Med. Eng. Phys.* **2005**, *27*, 221−228.
(49) Rojaee, M.; Fathi, K.; Raeissi. Electrophoretic deposition of nanostructured hydroxyapatite coating on AZ91 magnesium alloy implants with different surface treatments. *Appl. Surf. Sci.* **2013**, *285*, 664−673.
(50) Boccaccini, A. R.; Keim, S.; Ma, R.; Li, Y.; Zhitomirsky, I. Electrophoretic deposition of biomaterials. *Roy Soc. Interface.* **2010**, *7*, S581−S613.
(51) Maleki-Ghaleh, H.; Khalili, V.; Khalil-Allafi, J.; Javidi, M. Hydroxyapatite coating on NiTi shape memory alloy byelectrophoretic deposition process. *Surf. Coat. Technol.* **2012**, *208*, 57−63.
(52) de Groot, K.; Wolke, J. G. C.; Jansen, J. A. Calcium phosphate coatings for medical implants. *Proc. Inst. Mech. Eng., Part H* **1998**, *212*, 137−147.
(53) Herrera, A.; Mateo, J.; Gil-Abrova, J.; Lobo-Escolar, A.; Ibarz, E.; Gabarre, S.; Mas, Y.; Gracia, L. Clinical Study, Cementless Hydroxyapatite Coated Hip Prostheses. *BioMed Res. Int.* **2015**, *2015*, 386461.
(54) Geesink, R. G. T.; de Groot, K.; Klein, C. P. A. T. Bonding of bone to apatite-coated implants. *J. Bone Jt. Surg., Br. Vol.* **1988**, *70B* (1), 17−23.
(55) Röhrl, S. M. Wear and fixation of the acetabular component. In vivo evaluation of different polyethylenes and modes of fixation in total hip arthroplasty. Ph.D. Thesis, Umeå University, Umeå, Sweden, 2004.
(56) Yoshinari, M.; Matsuzaka, K.; Inoue, T.; Oda, Y.; Shimono, M. Bio-Functionalization of Titanium Surfaces for Dental Implants. *Mater. Trans.* **2002**, *43* (10), 2494−2501.
(57) Mohseni, E.; Zalnezhad, E.; Bushroa, A. R. Comparative investigation on the adhesion of hydroxyapatite coating on Ti-6Al-4V implant: A review paper. *Int. J. Adhes. Adhes.* **2014**, *48*, 238−257.
(58) Saber-Samandari, S.; Gross, K. A. Nanoindentation reveals mechanical properties within thermally sprayed hydroxyapatite coatings. *Surf. Coat. Technol.* **2009**, *203*, 1660−1664.
(59) Cheng, G. J.; Pirzada, D.; Cai, M.; Mohanty, P.; Bandyopadhyay, A. Bioceramic coating of hydroxyapatite on titanium substrate with Nd-YAG laser. *Mater. Sci. Eng., C* **2005**, *25* (4), 541−547.
(60) Rivera-Chacon, D. M.; Alvarado-Velez, M.; Acevedo-Morantes, C. Y.; Singh, S. P.; Gultepe, E.; Nagesha, D.; Sridhar, S.; Ramirez-Vick, J. E. Fibronectin and vitronectin promote human fetal osteoblast cell attachment and proliferation on nanoporous titanium surfaces. *J. Biomed. Nanotechnol.* **2013**, *9*, 1092−1097.
(61) Jeong, J.; Kim, J. H.; Shim, J. H.; Hwang, N. S.; Heo, C. Y. Bioactive calcium phosphate materials and applications in bone regeneration. *Biomaterials research.* **2019**, *23*, 4.
(62) Tian, Q.; Lin, J.; Rivera-Castaneda, L.; Tsanhani, A.; Dunn, Z. S.; Rodriguez, A.; Aslani, A.; Liu, H. Nano-to-submicron hydroxyapatite coatings for magnesium-based bioresorbable implants-deposition, characterization, degradation, mechanical properties, and cytocompatibility. *Sci. Rep.* **2019**, *9*, 1−27.
(63) Muthaiah, V. M. S.; Indrakumar, S.; Suwas, S.; Chatterjee, K. Surface engineering of additively manufactured titanium alloys for enhanced clinical performance of biomedical Implants: A review of recent developments. *Bioprinting* **2022**, *25*, e00180.

https://doi.org/10.1021/acsmaterialsau.1c00043
ACS Mater. Au 2022, 2, 132−142